Long-range electron correlation in dissociative double ionization of argon dimers

Hao Huang, Hongcheng Ni,* Jian Wu, Yan Yang, Junyang Ma,† and Zhenrong Sun
State Key Laboratory of Precision Spectroscopy, East China Normal University, Shanghai 200241, China

(Received 24 April 2025; accepted 15 July 2025; published 28 July 2025)

We experimentally investigate long-range electron-electron correlation across the two atomic sites of an argon dimer in its dissociative double ionization induced by a linearly polarized 400-nm femtosecond laser field. The correlation between the two electrons, ionized at two atomic sites, is revealed through analysis of the joint kinetic energy spectra and the momentum distributions. Notably, one of the two electrons exhibits a pronounced redshift in the low-kinetic-energy region, in contrast to the electron energy spectrum observed in single ionization of argon dimers. This distinctive spectral feature is corroborated by theoretical simulations, which attribute the redshift to the differing intensity dependence of the kinetic energy distributions of the two electrons, as well as to the influence of electron-electron correlation during the ionization process.

DOI: 10.1103/vm2r-127c

I. INTRODUCTION

When molecules are subjected to intense laser fields, they can undergo double ionization followed by rapid fragmentation, a process that is fundamental to ultrafast dynamics in physics and chemistry. A key mechanism underlying such processes is electron-electron correlation, which governs how electrons interact and share energy during strong-field ionization [1–7]. Over the past decades, a wide range of experimental and theoretical studies have demonstrated the essential role of electron correlation in molecular double ionization, revealing a diversity of ionization mechanisms and intricate energy redistribution pathways [8–14]. Advances in attosecond science have revealed quantum entanglement, which is an extreme manifestation of electron correlation, as a crucial phenomenon in strong-field processes, as demonstrated in recent studies [15–17]. In the multiphoton regime, femtosecond laser pulses can trigger nonsequential double ionization, wherein two electrons are ejected in a strongly correlated manner [18–23]. This process is typically initiated by the rescattering of the first ionized electron, which, driven back by the laser field, collides with and liberates a second electron [24–27]. For example, in above-threshold double ionization of acetylene [8], the absorption of multiple photons results in the emission of two electrons, with the excess energy shared between them. Such energy sharing can be directly observed in joint kinetic energy spectra, which often exhibit discrete diagonal structures indicative of correlated emission.

Compared to covalently bound molecules, gas-phase dimers offer a particularly advantageous platform for probing electron-electron correlation due to their extended internuclear separation [28,29]. This structural feature enables the study of long-range interactions between electrons localized on different atomic sites. For instance, in helium dimers, both theoretical and experimental investigations have demonstrated that single-photon double ionization leads to pronounced electron correlation, characterized by preferential back-to-back electron emission [30–32]. This emission pattern reflects the so-called knock-off mechanism, wherein a fast electron ejects a second electron through a binary encounter. Beyond such direct ionization pathways, intermolecular Coulombic decay further exemplifies the importance of correlation in weakly bound systems [33–37]. In intermolecular Coulombic decay, inner-shell ionization leaves the system in an excited state, which subsequently relaxes by transferring energy to a neighboring atom, resulting in the emission of a low-energy electron. These diverse mechanisms collectively underscore the fundamental role of electron correlation in multielectron processes and motivate continued investigation into correlated dynamics in complex molecular systems. However, despite significant progress in understanding strong-field ionization of simple molecules [38], the role of electron-electron correlation in the multiphoton double ionization of gas-phase dimers, particularly in the above-threshold regime, remains largely unexplored.

In this work we investigate the dissociative double ionization of argon dimers (with electrons released from different atomic sites) driven by a linearly polarized 400-nm femtosecond laser field, with a joint experimental-theoretical study employing coincident detection and time-dependent Schrödinger equation (TDSE) simulations. The measured kinetic energy release spectra of the ionic fragments confirm a two-center fragmentation mechanism, with negligible correlation between the energies of the emitted electrons and the ionic fragments. However, analysis of the joint kinetic energy spectra and momentum distributions of the electrons reveals delicate electron-electron correlation. In particular, one of the electrons exhibits a redshift in its kinetic energy spectra relative to electrons emitted in single ionization. This redshifted spectral feature is consistently reproduced by TDSE simulations and is attributed to two key factors: the different dependence of the temporally ordered emitted electrons on laser intensity and the strong modulation of energy-sharing dynamics mediated by electron-electron correlation. These

*Contact author: hcni@lps.ecnu.edu.cn
†Contact author: jyma@lps.ecnu.edu.cn

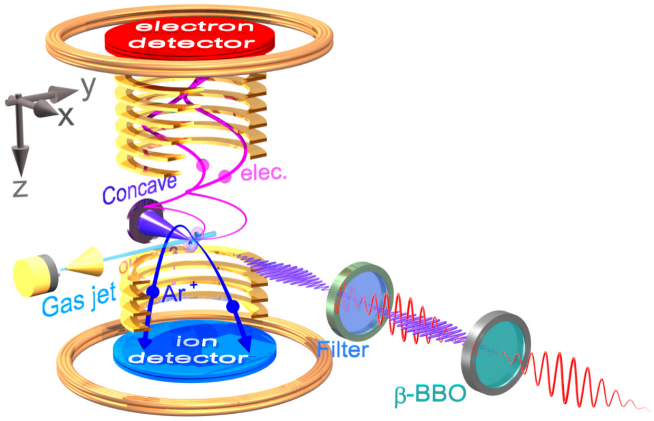

FIG. 1. Schematic diagram of the experimental setup.

findings provide new insights into the interplay between strong-field ionization dynamics and electron-electron correlation in weakly bound systems.

The article is organized as follows. In Sec. II we present the experimental setup. In Sec. III we detail the theoretical method. In Sec. IV we demonstrate the experimentally measured results and the corresponding theoretical simulations. A summary is given and conclusions are discussed in Sec. V. Hartree atomic units $e = m_e = \hbar = 1$ are used throughout the article unless stated otherwise.

II. EXPERIMENTAL SETUP

A coincident measurement of two photoelectrons and two ionic fragments resulting from the dissociative double ionization of argon dimers was conducted using a cold-target recoil-ion momentum spectroscopy apparatus [39], as schematically illustrated in Fig. 1. The laboratory coordinate system is defined with the y axis aligned with the supersonic gas jet propagation, the z axis oriented along the time-of-flight direction, and the x axis coinciding with the laser propagation direction. A femtosecond laser pulse, linearly polarized along the y axis with a central wavelength of 400 nm, was generated by frequency doubling a near-infrared pulse (25 fs, 800 nm, 10 kHz) from a Ti:sapphire laser system in a 200-μm-thick β-barium borate crystal. After filtering out the residual 800-nm component, the 400-nm laser pulse was tightly focused onto a supersonic argon gas beam using a concave mirror. The peak laser intensity was determined through a careful calibration procedure based on the measured yield ratio of Ar^{2+} to Ar^{+} ions, following the procedure described in Ref. [23]. This approach yielded an estimated peak intensity of 8×10^{13} W/cm^2 in the interaction region. The temporal duration of the laser pulse was 50 fs. The Keldysh parameter for argon dimers was estimated to be greater than 1, indicating that the experiment was conducted in the multiphoton ionization regime. The resulting ionic fragments and photoelectrons were accelerated and guided by a weak static electric field (11.1 V/cm) and a magnetic field (10.5 G) within the spectrometer, enabling their detection in coincidence using two time- and position-sensitive microchannel plate detectors located at opposite ends of the spectrometer. The kinetic energies of the detected ionic fragments and photoelectrons were reconstructed based on their measured time of flight and impact positions. Under our experimental conditions, the argon dimer concentration in the supersonic jet is typically 1% of the monomer density, as determined from the Ar^{+}/Ar^{2+} ion yield ratio. Given the measured monomer ionization probability of 0.1 per laser pulse at 10-kHz repetition rate, we estimate a corresponding dimer ionization rate of about ten events per second. To suppress false coincidences while preserving sufficient data statistics, the ion-to-electron count ratio was maintained at 1:1.2. Additionally, a momentum gating condition was applied during data analysis, requiring the total momentum of the two detected ions and two electrons to be less than 0.5 a.u., thereby ensuring consistency with overall momentum conservation in the dissociative double ionization of argon dimers.

III. THEORETICAL METHOD

In argon dimers interacting with a linearly polarized laser field, the ion pair angular distribution peaks along the laser polarization direction [29]. This suggests that the dominant dynamics can be modeled by aligning the dimer axis with the laser polarization. Since the laser-driven electron motion is primarily confined to this direction as well, our simulations employ a two-dimensional two-electron TDSE within a double-well model potential [40,41], where each electron is restricted to one dimension. While this approach neglects motion perpendicular to the polarization axis, it significantly enhances computational efficiency while retaining the essential physics of two-electron dynamics driven by the laser field. In this way, we aim to reconstruct the interaction between linearly polarized laser pulses and argon dimers theoretically. It is further assumed that the emission of the electron proceeds fast enough to keep the internuclear distance of the two atoms fixed during the simulations, which is supported by the subsequent experiment results. Thus, the two-dimensional model Hamiltonian is given by [32]

$$H = \frac{p_1^2}{2} + \frac{p_2^2}{2} + \frac{1}{R} + F(t)(y_1 + y_2) + V_{\mathrm{SAE}}(r_{11}) + V_{\mathrm{SAE}}(r_{12}) + V_{\mathrm{SAE}}(r_{21}) + V_{\mathrm{SAE}}(r_{22}) + \frac{1}{\sqrt{(y_1 - y_2)^2 + b^2}}, \quad (1)$$

where p_i and y_i (with $i = 1, 2$) are the momentum operators and spatial coordinates of the two active electrons. The linearly polarized laser field is given in the form of

$$F(t) = F_0 \cos^2\left(\frac{\omega t}{2N}\right) \sin(\omega t + \phi), \quad (2)$$

where ω is the central frequency corresponding to a wavelength of 400 nm, N is the number of cycles, and $\phi = 0$ is the carrier-envelope phase of the laser pulse. The potential terms in our simulation employ distinct soft-core parameters for different interactions. The electron-ion interaction is given by the single-active-electron potential for argon

$$V_{\mathrm{SAE}}(r) = -\frac{Z_c + a_1 e^{-a_2 r^2}}{r}, \quad (3)$$

with $Z_c = 1.0$, $a_1 = 0.1215$, and $a_2 = 0.0362$. The distance between the ith electron and jth nucleus ($i, j = 1, 2$) is

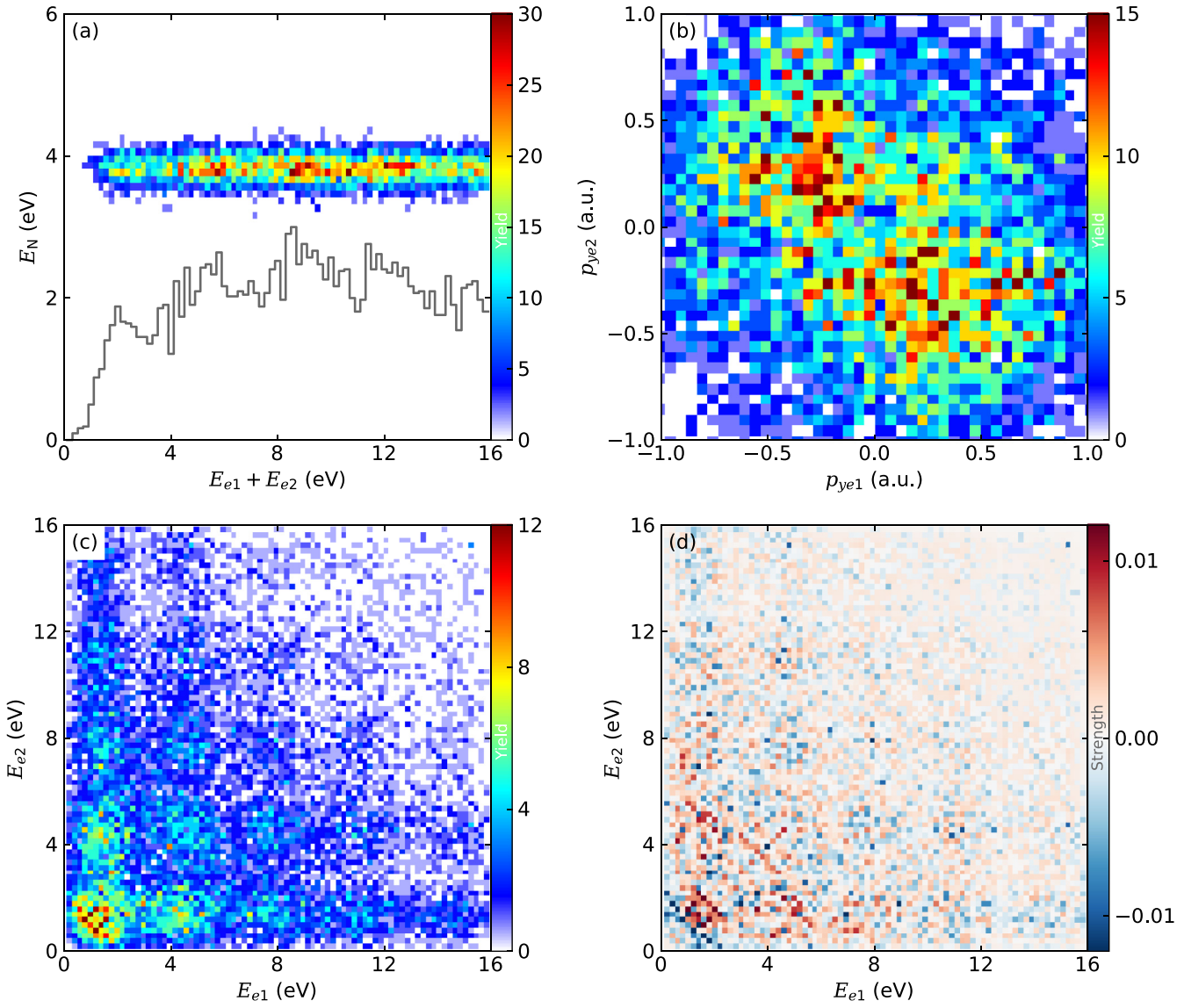

FIG. 2. (a) Joint energy spectra of the two electrons and two ionic fragments. The gray step line corresponds to the scaled sum kinetic energy spectra of the two electrons. (b) Joint momentum distribution along the laser polarization direction and (c) kinetic energy spectra of the two electrons. (d) Correlation analysis based on the joint kinetic energy spectra.

given by

$$r_{ij} = \{[y_i + (-1)^j R/2]^2 + a^2\}^{1/2}, \tag{4}$$

where $a^2 = 1.9$ is the electron-ion soft-core parameter and the internuclear separation $R = 7.16$ a.u. corresponds to the equilibrium position of the neutral argon dimer potential [42]. The electron-electron interaction, on the other hand, is given by the Coulomb-repulsion potential $1/\sqrt{(y_1 - y_2)^2 + b^2}$, where $b^2 = 10$ is the electron-electron soft-core parameter. With these parameters, the ionization potentials of the two active electrons are comparable to the experimental values. Since the motion of electrons is confined to one dimension, the electron-electron interaction and electron-nuclei interaction are significantly overestimated, necessitating the usage of large values of the soft-core parameters to counter the impact of dimensionality reductions.

IV. RESULTS AND DISCUSSION

Figure 2(a) presents the joint energy spectra of the two electrons and two ionic fragments resulting from the dissociative double ionization of argon dimers. In this plot, $E_{e1} + E_{e2}$ denotes the total kinetic energy of the two electrons, while E_N represents the total kinetic energy of the two ionic fragments. The absence of photon-energy-spaced diagonal structures suggests that electron-nuclear correlation is weak. The measured value of $E_N = 3.8$ eV agrees well with the Coulomb repulsion energy estimated by $E_N = 1/R$, where $R = 7.16$ a.u. is the equilibrium internuclear distance of the neutral argon dimer [42]. This agreement indicates that the dimer undergoes prompt Coulomb explosion following a two-site double ionization, without appreciable nuclear motion between the two ionization steps. As a result, electron-nuclear energy correlation is negligible. Notably, the electron sum kinetic energy spectrum exhibits multiple peaks spaced by

the photon energy, evidencing that the absorbed photons are shared between the two electrons. In the presence of intense femtosecond laser fields, molecules can absorb more photons than required for ionization, leading to above-threshold double ionization [43,44] and resulting in discrete peaks in the electron energy spectrum.

To further investigate electron-electron correlation, we examine the joint momentum distribution along the laser polarization direction and the kinetic energy spectra of the two electrons, shown in Figs. 2(b) and 2(c), respectively. In Fig. 2(b), a clear anticorrelation is observed, with a higher density of events in the second and fourth quadrants for the low-energy part of the spectrum. This back-to-back emission pattern indicates that the electrons are preferentially ejected in opposite directions when they possess low kinetic energies, a hallmark of correlated double-ionization dynamics [45–47]. Further insights into back-to-back emission are provided in Appendix B. The joint kinetic energy spectrum in Fig. 2(c), which displays structured features rather than a featureless background (as seen in helium [48]), further confirms the presence of clear electron-electron correlation. To quantify this, we performed a correlation analysis shown in Fig. 2(d). The joint energy distribution $P(E_{e1}, E_{e2})$ was integrated along each axis to obtain the individual energy distributions $P(E_{e1})$ and $P(E_{e2})$. The correlation signal was then constructed by subtracting the normalized joint distribution $P(E_{e1}, E_{e2})$ from the uncorrelated product $P(E_{e1}) \otimes P(E_{e2})$. A clear correlation is evident in the region where the differences is nonzero. Remarkably, the correlation is pronounced at low-energy regions and diminishes with increasing energy. Further insights into electron-electron correlation are provided in Appendix A, where we compare joint kinetic energy spectra of electron pairs emitted in the same versus opposite directions. Their joint energy distributions exhibit distinct differences depending on their relative emission angles, underscoring the role of electron-electron interactions in shaping the final energy-sharing dynamics. These results demonstrate that, in the multiphoton double ionization of argon dimers, the two emitted electrons exhibit discernible correlation in both energy and momentum, providing new insight into strong-field ionization dynamics in weakly bound systems.

Interestingly, a redshift is observed in the experimentally measured energy distribution of one of the two electrons from the dissociative double ionization of argon dimers, compared to that from single ionization, as shown in Fig. 3(a). Specifically, the first above-threshold ionization (ATI) peak exhibits a shift of approximately 0.4 eV. Notably, the observed order-dependent attenuation of the redshift effect [Fig. 3(a)] is not rooted in intensity averaging, where uniform ponderomotive shifts should preserve relative peak spacings across all ATI orders. To verify this behavior, we numerically solved the time-dependent Schrödinger equation using a laser field with the same intensity and a pulse duration corresponding to $N = 24$ optical cycles. The double-ionization signal was extracted by removing the bound and single-ionization part of the wave function via setting the final wave function to zero in regions where any of the following conditions were met: $r_{11} < 40$ a.u., $r_{22} < 40$ a.u., $r_{12} < 40$ a.u., or $r_{21} < 40$ a.u. After Fourier transformation and integrating over the momentum coordinate of one electron, the energy distribution of a single electron from the double-ionization process was obtained [red curve in Fig. 3(b)]. For comparison, the single-ionization spectrum was computed by removing the wave function in the region $r_{11} < 40$ a.u. or $r_{22} > 40$ a.u. All spectra in Fig. 3 are normalized, and the red curves corresponding to double ionization are vertically shifted by 0.2 for better visibility. Overall, the simulation agrees with the experimental data. The energy difference between the first ATI peaks in the simulated single- and double-ionization spectra matches the experimentally observed redshift. This redshift also decreases at higher electron energies, supporting the validity of the theoretical model. The Coulomb interaction between the electrons was softened using a large soft-core parameter to better mimic the three-dimensional case. Nevertheless, a pronounced redshift remains in the calculated energy distribution, reflecting the long-range correlation between the two electrons. Some discrepancies are expected due to the dimensionality reduction, which results in stronger laser-electron interaction compared to the actual experiment. The double-ionization probability is extracted from the final wave function by the criterion when both electrons are located beyond 40 a.u. from the ionic cores. While this criterion successfully captures direct double-ionization events, it also includes contributions from mixed states where one electron is ionized while the other occupies high Rydberg orbitals. This inclusion accounts for the additional side peaks present in our theoretical spectra that are not observed experimentally.

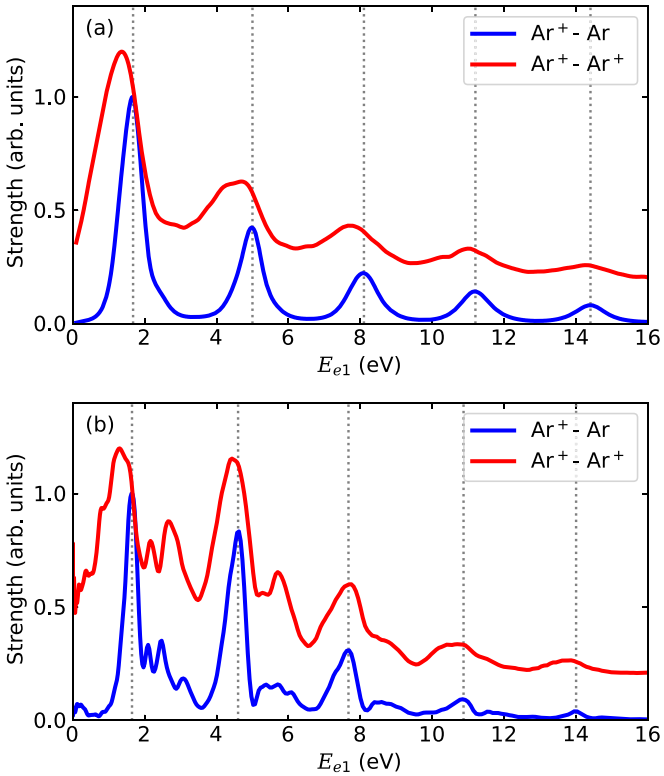

FIG. 3. (a) Experimentally measured and (b) theoretically simulated energy distribution of one electron from double ionization of argon dimers and that from single ionization of argon dimers at 8×10^{13} W/cm^2. The gray dotted lines denote the peak positions of the electron energy distribution for single ionization.

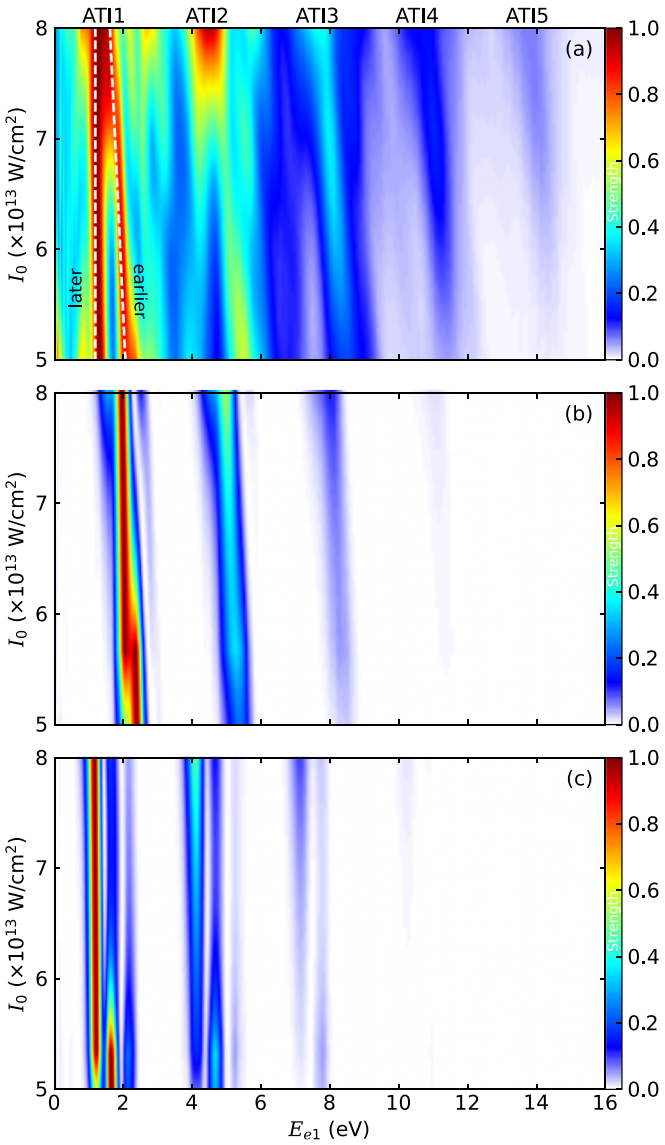

FIG. 4. Normalized energy distribution of one of the electrons emitted in the double ionization as a function of the laser intensity calculated with (a) the full model Hamiltonian and with the reduced Hamiltonians (b) H_1 [Eq. (5)] and (c) H_2 [Eq. (6)]. Different ATI regions are marked at the top of the figure.

To investigate the origin of the redshift in Fig. 3, we calculated the energy distribution of one electron from double ionization as a function of laser intensity ranging from 5×10^{13} to 8×10^{13} W/cm^2 with the full Hamiltonian, as shown in Fig. 4(a). In the range of 1.0–2.2 eV pertaining to ATI1 as marked in the figure, two distinct peaks are observed, where the higher-energy peak corresponds to the earlier-emitted electron and the lower-energy peak corresponds to the later-emitted electron. This distinction arises from their different ionization potential energies $I_p^{\text{earlier}} = 15.8$ eV and $I_p^{\text{later}} = 19.8$ eV and different numbers of absorbed photons $N_{\text{earlier}} = 6$ and $N_{\text{later}} = 7$. The calculated ionization potentials of 15.8 eV (Ar atom) and 19.8 eV (Ar dimer cation) are obtained by solving the eigenvalue problem for our model system's initial wave functions. These values show excellent agreement with those reported in Ref. [29] (15.76 and 19.54 eV, respectively). Therefore, the energy of the two electrons in the ATI1 region can be defined as $E_{\text{earlier}} = N_{\text{earlier}}\omega - I_p^{\text{earlier}} - U_p^{\text{earlier}} = 2.8$ eV $-U_p^{\text{earlier}}$ and $E_{\text{later}} = N_{\text{later}}\omega - I_p^{\text{later}} - U_p^{\text{later}} = 1.9$ eV $-U_p^{\text{later}}$, respectively. An energy difference of 0.9 eV can be observed between the two electrons when their ponderomotive potentials are equal. The same interpretation applies to higher-order peaks. As laser intensity increases, the energy distribution of the earlier-emitted electron redshifts due to the varying ponderomotive potential U_p^{earlier}. However, the energy distribution of the later-emitted electron in ATI1 region barely moves, apparently due to the presence of Freeman resonance [49] through intermediate Rydberg states in the ionization process.

At 8×10^{13} W/cm^2, the peaks from both electrons overlap and form a new composite set of peaks as an entirety, shown in Fig. 3(b) and the top region of Fig. 4(a). In the ATI1 region, the peak position of the earlier-emitted electron is 1.7 eV at 8×10^{13} W/cm^2 ($U_p^{\text{earlier}} = 1.1$ eV), while the peak position of the later-emitted electron is fixed at 1.2 eV. As the signal strength of the later-emitted electron in the ATI1 region is significantly enhanced by Freeman resonance, the position of the ATI1 peak closely aligns with that of the later-emitted electron, showing an approximately 0.4-eV deviation from the 1.7-eV peak position characteristic of the earlier-emitted electron. Conversely, for higher-order ATI peaks, the signal is predominantly governed by the earlier-emitted electron, as the later-emitted electron in the same ATI region must absorb an additional photon, thereby reducing their respective probability. Thus the postions of the higher-order ATI peaks closely align with those of the earlier-emitted electron, causing the absence of a clear redshift in higher-order ATI peaks.

To distinguish the effects of different correlation effects in the resulting spectra, we carried out the calculations using reduced Hamiltonians [32], where certain interaction terms are removed from the full Hamiltonian to isolate their respective roles. The Hamiltonian reduction is particularly applicable for the dimer system because the removal of individual interaction terms does not significantly impact the initial distribution of the wave function due to large spatial separation of the two atomic sites. For the earlier-emitted electron, the dynamics are primarily governed by the Coulomb potential of its parent nucleus and the external laser field. At this stage, the influence of neighboring neutral argon atom is negligible due to the relatively large internuclear distance that weakens direct Coulomb interactions with the neutral neighbor. This justifies the reduced form of the Hamiltonian

$$H_1 = \frac{p_1^2}{2} + \frac{p_2^2}{2} + \frac{1}{R} + F(t)(y_1 + y_2) + V_{\text{SAE}}(r_{11}) + V_{\text{SAE}}(r_{22}) \tag{5}$$

used in Fig. 4(b), which effectively captures the essential two-body interaction between the electron and its parent ion. As laser intensity increases, the ponderomotive potential increases, leading to an overall redshift of the photoelectron energy distribution. Such a redshift is consistent with the signal of the earlier-emitted electron shown in Fig. 4(a), as both arise from this dominant physical picture. Following the

departure of the first electron, the later emitted electron encounters a significantly altered potential landscape. It is now subject to the Coulomb fields of both the parent ion and the neighboring ionized argon atom, in addition to the laser field. The presence of the second ion introduces a non-negligible multicenter Coulomb interaction that must be accounted for in the theoretical description. Therefore, in Fig. 4(c) the reduced Hamiltonian

$$H_2 = \frac{p_1^2}{2} + \frac{p_2^2}{2} + \frac{1}{R} + F(t)(y_1 + y_2) + V_{\mathrm{SAE}}(r_{11}) + V_{\mathrm{SAE}}(r_{12}) + V_{\mathrm{SAE}}(r_{21}) + V_{\mathrm{SAE}}(r_{22}) \quad (6)$$

incorporates additional terms from the full Hamiltonian (1) to properly describe this more complex scenario. This treatment explains why the signal in Fig. 4(c) parallels that of the later electron in Fig. 4(a), where the electron's motion is influenced by the combined potential of the two ions.

If there is negligible interaction between the two active electrons in the argon dimer, their respective ATI signals in Fig. 4(a) should be similar to those in Figs. 4(b) and 4(c), respectively. However, this is not the case; the long-range electron-electron interaction exhibits a modulation of the double ionization process. Freeman resonances can be observed more clearly in both Figs. 4(b) and 4(c), while their dependence on intensity differs. In Fig. 4(b), as the ponderomotive potential increases with the laser intensity, different intermediate states successively dominate the resonance process. In Fig. 4(c) the original ATI peaks split into a series of narrow peaks, which correlate with their corresponding intermediate states. Since the peak in the ATI1 region lies closest to the peak arising from these intermediate states, the signal consequently experiences a marked enhancement, accounting for the redshift depicted in Fig. 3(b). However, the inclusion of electron-electron interaction in the full Hamiltonian modifies the intermediate resonance states of the earlier-emitted electron, suppressing its Freeman resonances seen in Fig. 4(b). In contrast, for the later-emitted electron, these structures remain visible since the earlier-emitted electron has already departed. Additionally, the energy peaks in Fig. 4(a) are broader than those in Figs. 4(b) and 4(c), highlighting the role of long-range electron-electron interaction in shaping the ATI structure and contributing to the observed redshift.

V. CONCLUSION

In summary, we have demonstrated the presence of long-range electron-electron correlation in the multiphoton double ionization of argon dimers through the experimentally measured electron-electron joint momentum and kinetic energy spectra. A redshift was observed in the energy distribution of one of the electrons from the double-ionization process, in contrast to that from single ionization. This phenomenon was reproduced by two-dimensional TDSE simulations. By calculating the electron energy distributions as a function of laser intensity using various model Hamiltonians, we confirmed that the distinct intensity dependence of the two temporally ordered ionized electrons, along with the modulation by electron-electron correlation, is the underlying cause of the redshift. This work provides deeper insight into long-range electron correlation effects in multiphoton double-ionization processes of noble-gas dimers and lays the groundwork for future studies on ultrafast electron dynamics in extended systems.

ACKNOWLEDGMENTS

This work was supported by the Innovation Program for Quantum Science and Technology (Grant No. 2024ZD0300700), the National Natural Science Fund of China (Grants No. 92461301, No. 12204175, No. 12034008, No. 12250003, No. 12474341, No. 12227807, and No. 12241407), the Shanghai Pujiang Program (Grant No. 24PJA025), the Science and Technology Commission of Shanghai Municipality (Grant No. 23JC1402000), and the Shanghai Pilot Program for Basic Research (Grant No. TQ20240204). Numerical computations were in part performed on the ECNU Multifunctional Platform for Innovation (001).

DATA AVAILABILITY

The data that support the findings of this article are openly available [50].

APPENDIX A: ELECTRON-ELECTRON JOINT KINETIC ENERGY SPECTRA IN DIFFERENT QUADRANTS

Figure 5 presents the experimentally measured joint kinetic energy distributions of the two electrons from double ionization, with Fig. 5(a) showing electrons emitted in the same direction and Fig. 5(b) displaying electrons emitted back to back. These measurements reveal distinct energy correlation patterns for the two emission geometries. Specifically, the energy distribution in Fig. 5(a) exhibits concentration along the diagonal extremes (highlighted with a black dashed line) in region where the energies of both emitted electrons are below 2 eV, compared with Fig. 5(b), which features mainly grid-line distribution (highlighted with white dashed lines). This means that the energy difference between the two electrons is significantly larger when they are emitted in the same direction. This can be attributed to the stronger Coulomb interaction experienced when both electrons are emitted in the same direction

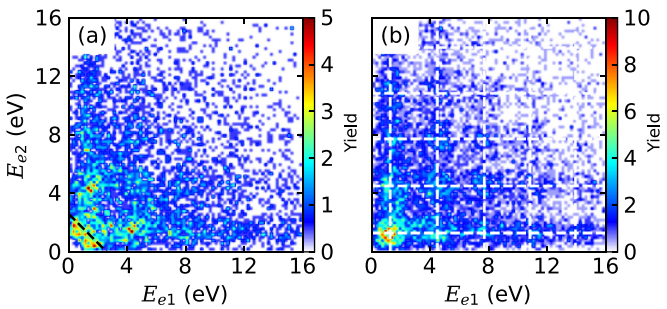

FIG. 5. Experimentally measured joint kinetic energy spectra of the two electrons emitted in the (a) same and (b) opposite directions, where the momentum vectors of the two electrons are the same or opposite along the laser polarization direction, respectively. In addition, the black and white dashed lines indicate the primary features of the signals in (a) and (b), respectively.

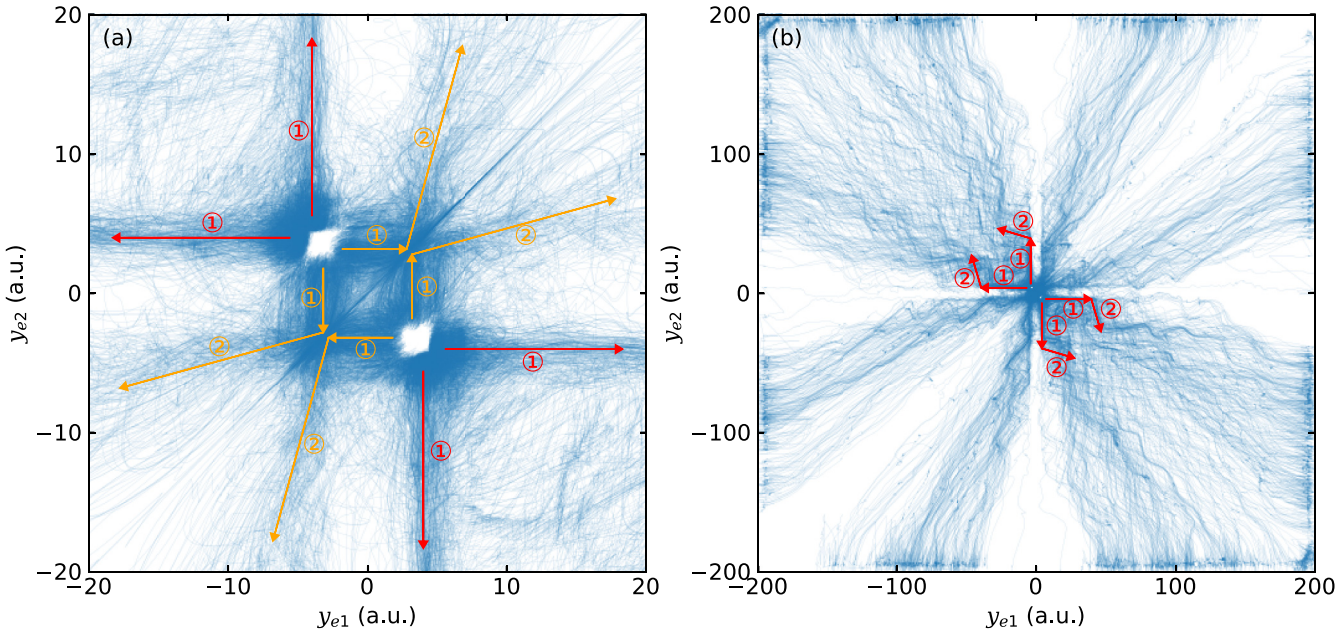

FIG. 6. Trajectories leading to double ionization of the argon dimer shown in the ranges (a) $y_{e1}, y_{e2} \in [-20, 20]$ and (b) $y_{e1}, y_{e2} \in [-200, 200]$. Orange and red arrows represent electron emission in the same and opposite directions, respectively. Steps ① and ② indicate electron emission one after the other.

with relatively low velocities, resulting in mutual repulsion: One electron is decelerated while the other is accelerated. In contrast, when the electrons are emitted in opposite directions, they quickly separate, reducing the influence of Coulomb repulsion and leading to a smaller energy difference between them. This directional dependence of the joint kinetic energy spectra highlights the role of electron-electron interaction in shaping the final energy sharing between the two ionized electrons.

APPENDIX B: BOHMIAN MECHANICS

To elucidate the origin of the back-to-back emission shown in Fig. 2(b) and the role of electron scattering, we perform simulations of the emission process using Bohmian mechanics [51,52]. This approach provides a trajectory-based interpretation of quantum dynamics, where the initial positions of the trajectories (y_1, y_2) are sampled from the initial two-electron wave function, localized around the coordinate $(-R/2, R/2)$ and its symmetric counterpart $(R/2, -R/2)$. The evolution of these trajectories is governed by the equation of motion

$$m\dot{\boldsymbol{r}} = \nabla S(\boldsymbol{r}, t), \tag{B1}$$

where $S(\boldsymbol{r}, t) = \arg \psi(\boldsymbol{r}, t)$ is the time-dependent phase of the wave function obtained from the solution of the TDSE.

All trajectories leading to double ionization of the argon dimer are depicted in Fig. 6. The orange and red arrows distinguish between nonsequential (same-direction emission) and sequential (opposite-direction emission) ionization pathways, respectively. For both pathways, the process occurs in two distinct steps ① and ②. In the nonsequential pathway (orange arrows), the first ionized electron moves toward the neighboring argon atom, liberating the second electron via scattering. The two electrons then propagate in the same direction but with a significant velocity difference. The histogram between their emission times reveals that the rescattering process typically take three to five optical cycles. Conversely, in the sequential pathway (red arrows), the first electron moves away from the dimer, while the second electron is predominantly emitted in the opposite direction, resulting in back-to-back ionization. Unlike the nonsequential case, the second electron can be emitted at any time during the pulse [Fig. 6(b)]. The asymmetry between the two pathways arises from (i) the Coulomb repulsion between the electrons and (ii) the trapping of the second electron by the Coulomb potential of the neighboring nucleus, which suppresses emission in the direction of the first electron. In addition, Fig. 6(b) demonstrates that trajectories corresponding to back-to-back emission (second and fourth quadrants) are more abundant and clustered near the diagonal, indicating a smaller momentum difference between the electrons compared to same-direction emission (first and third quadrants). This aligns with the experimental observations in Fig. 5.

[1] A. Talebpour, S. Larochelle, and S.-L. Chin, Non-sequential and sequential double ionization of NO in an intense femtosecond Ti:sapphire laser pulse, J. Phys. B **30**, L245 (1997).

[2] C. Cornaggia and P. Hering, Laser-induced non-sequential double ionization of small molecules, J. Phys. B **31**, L503 (1998).

[3] J. Wu, H. Zeng, and C. Guo, Polarization effects on nonsequential double ionization of molecular fragments in strong laser fields, Phys. Rev. A **75**, 043402 (2007).

[4] P. Lablanquie, T. P. Grozdanov, M. Žitnik, S. Carniato, P. Selles, L. Andric, J. Palaudoux, F. Penent, H. Iwayama, E. Shigemasa, Y. Hikosaka, K. Soejima, M. Nakano, I. H. Suzuki, and K. Ito, Evidence of single-photon two-site core double ionization of C_2H_2 molecules, Phys. Rev. Lett. **107**, 193004 (2011).

[5] Y. Li, S. Yang, J. Chen, and J. Fan, Non-sequential double ionization of diatomic molecules: Alignment dependence of electron correlation, J. Phys. B **47**, 045601 (2014).

[6] M. Kübel, K. J. Betsch, N. G. Kling, A. S. Alnaser, J. Schmidt, U. Kleineberg, Y. Deng, I. Ben-Itzhak, G. G. Paulus, T. Pfeifer, J. Ullrich, R. Moshammer, M. F. Kling, and B. Bergues, Nonsequential double ionization of Ar: From the single- to the many-cycle regime, New J. Phys. **16**, 033008 (2014).

[7] K. Lin, X. Chen, S. Eckart, H. Jiang, A. Hartung, D. Trabert, K. Fehre, J. Rist, L. P. H. Schmidt, M. S. Schöffler, T. Jahnke, M. Kunitski, F. He, and R. Dörner, Magnetic-field effect as a tool to investigate electron correlation in strong-field ionization, Phys. Rev. Lett. **128**, 113201 (2022).

[8] X. Gong, Q. Song, Q. Ji, K. Lin, H. Pan, J. Ding, H. Zeng, and J. Wu, Channel-resolved above-threshold double ionization of acetylene, Phys. Rev. Lett. **114**, 163001 (2015).

[9] A. H. Winney, Y. F. Lin, S. K. Lee, P. Adhikari, and W. Li, State-resolved three-dimensional electron-momentum correlation in nonsequential double ionization of benzene, Phys. Rev. A **93**, 031402(R) (2016).

[10] Q. Song, P. Lu, X. Gong, Q. Ji, K. Lin, W. Zhang, J. Ma, H. Zeng, and J. Wu, Dissociative double ionization of CO in orthogonal two-color laser fields, Phys. Rev. A **95**, 013406 (2017).

[11] P. Lu, W. Zhang, X. Gong, Q. Song, K. Lin, Q. Ji, J. Ma, F. He, H. Zeng, and J. Wu, Electron-nuclear correlation in above-threshold double ionization of molecules, Phys. Rev. A **95**, 033404 (2017).

[12] W. Zhang, Z. Yu, X. Gong, J. Wang, P. Lu, H. Li, Q. Song, Q. Ji, K. Lin, J. Ma, H. Li, F. Sun, J. Qiang, H. Zeng, F. He, and J. Wu, Visualizing and steering dissociative frustrated double ionization of hydrogen molecules, Phys. Rev. Lett. **119**, 253202 (2017).

[13] C. Cheng, P. Vindel-Zandbergen, S. Matsika, and T. Weinacht, Electron correlation in channel-resolved strong-field molecular double ionization, Phys. Rev. A **100**, 053405 (2019).

[14] Z. Guo, Z. Zhang, Y. Deng, J. Wang, D. Ye, J. Liu, and Y. Liu, Probing H_2 double ionization with bicircular laser fields, Phys. Rev. Lett. **132**, 143201 (2024).

[15] M. J. J. Vrakking, Control of attosecond entanglement and coherence, Phys. Rev. Lett. **126**, 113203 (2021).

[16] A. S. Maxwell, L. B. Madsen, and M. Lewenstein, Entanglement of orbital angular momentum in non-sequential double ionization, Nat. Commun. **13**, 4706 (2022).

[17] S. Eckart, D. Trabert, J. Rist, A. Geyer, L. P. H. Schmidt, K. Fehre, and M. Kunitski, Ultrafast preparation and detection of entangled atoms, Sci. Adv. **9**, eabq8227 (2023).

[18] T. Weber, H. Giessen, M. Weckenbrock, G. Urbasch, A. Staudte, L. Spielberger, O. Jagutzki, V. Mergel, M. Vollmer, and R. Dörner, Correlated electron emission in multiphoton double ionization, Nature (London) **405**, 658 (2000).

[19] C. Cornaggia and P. Hering, Nonsequential double ionization of small molecules induced by a femtosecond laser field, Phys. Rev. A **62**, 023403 (2000).

[20] X. Liu, H. Rottke, E. Eremina, W. Sandner, E. Goulielmakis, K. O. Keeffe, M. Lezius, F. Krausz, F. Lindner, M. G. Schätzel, G. G. Paulus, and H. Walther, Nonsequential double ionization at the single-optical-cycle limit, Phys. Rev. Lett. **93**, 263001 (2004).

[21] B. Bergues, M. Kübel, N. G. Johnson, B. Fischer, N. Camus, K. J. Betsch, O. Herrwerth, A. Senftleben, A. M. Sayler, T. Rathje, T. Pfeifer, I. Ben-Itzhak, R. R. Jones, G. G. Paulus, F. Krausz, R. Moshammer, J. Ullrich, and M. F. Kling, Attosecond tracing of correlated electron-emission in non-sequential double ionization, Nat. Commun. **3**, 813 (2012).

[22] C. F. de Morisson Faria, T. Shaaran, and M. T. Nygren, Time-delayed nonsequential double ionization with few-cycle laser pulses: Importance of the carrier-envelope phase, Phys. Rev. A **86**, 053405 (2012).

[23] K. Henrichs, M. Waitz, F. Trinter, H. Kim, A. Menssen, H. Gassert, H. Sann, T. Jahnke, J. Wu, M. Pitzer, M. Richter, M. S. Schöffler, M. Kunitski, and R. Dörner, Observation of electron energy discretization in strong field double ionization, Phys. Rev. Lett. **111**, 113003 (2013).

[24] A. Becker, R. Dörner, and R. Moshammer, Multiple fragmentation of atoms in femtosecond laser pulses, J. Mod. Opt. **38**, S753 (2005).

[25] F. Krausz and M. Ivanov, Attosecond physics, Rev. Mod. Phys. **81**, 163 (2009).

[26] C. F. de Morisson Faria and X. Liu, Electron-electron correlation in strong laser fields, J. Phys. B **58**, 1076 (2011).

[27] W. Becker, X. Liu, P. J. Ho, and J. H. Eberly, Theories of photoelectron correlation in laser-driven multiple atomic ionization, Rev. Mod. Phys. **84**, 1011 (2012).

[28] B. Ulrich, A. Vredenborg, A. Malakzadeh, M. Meckel, K. Cole, M. Smolarski, Z. Chang, T. Jahnke, and R. Dörner, Double-ionization mechanisms of the argon dimer in intense laser fields, Phys. Rev. A **82**, 013412 (2010).

[29] B. Manschwetus, H. Rottke, G. Steinmeyer, L. Foucar, A. Czasch, H. Schmidt-Böcking, and W. Sandner, Mechanisms underlying strong-field double ionization of argon dimers, Phys. Rev. A **82**, 013413 (2010).

[30] T. Havermeier, T. Jahnke, K. Kreidi, R. Wallauer, S. Voss, M. Schöffler, S. Schössler, L. Foucar, N. Neumann, J. Titze, H. Sann, M. Kühnel, J. Voigtsberger, A. Malakzadeh, N. Sisourat, W. Schöllkopf, H. Schmidt-Böcking, R. E. Grisenti, and R. Dörner, Single photon double ionization of the helium dimer, Phys. Rev. Lett. **104**, 153401 (2010).

[31] H. Ni, C. Ruiz, R. Dörner, and A. Becker, Numerical simulations of single-photon double ionization of the helium dimer, Phys. Rev. A **88**, 013407 (2013).

[32] H. Ni and A. Becker, Theoretical analysis of the role of Coulomb interactions in single and double photoionization of the helium dimer using numerical model simulations, Phys. Rev. A **89**, 033402 (2014).

[33] S. Barth, S. Joshi, S. Marburger, V. Ulrich, A. Lindblad, G. Öhrwall, O. Björneholm, and U. Hergenhahn, Observation of resonant interatomic Coulombic decay in Ne clusters, J. Chem. Phys. **122**, 241102 (2005).

[34] P. O'Keeffe, E. Ripani, P. Bolognesi, M. Coreno, M. Devetta, C. Callegari, M. Di Fraia, K. C. Prince, R. Richter, M. Alagia,

A. Kivimäki, and L. Avaldi, The role of the partner atom and resonant excitation energy in interatomic Coulombic decay in rare gas dimers, J. Phys. Chem. Lett. **4**, 1797 (2013).

[35] M. Kimura, H. Fukuzawa, T. Tachibana, Y. Ito, S. Mondal, M. Okunishi, M. Schöffler, J. Williams, Y. Jiang, Y. Tamenori, N. Saito, and K. Ueda, Controlling low-energy electron emission via resonant-Auger-induced interatomic Coulombic decay, J. Phys. Chem. Lett. **4**, 1838 (2013).

[36] T. Jahnke, U. Hergenhahn, B. Winter, R. Dörner, U. Frühling, P. V. Demekhin, K. Gokhberg, L. S. Cederbaum, A. Ehresmann, A. Knie, and A. Dreuw, Interatomic and intermolecular Coulombic decay, Chem. Rev. **120**, 11295 (2020).

[37] A. Hans, F. Trinter, P. Schmidt, S. Eckart, S. Grundmann, G. Hartmann, X. Holzapfel, C. Honisch, G. Kastirke, M. Kircher, N. Melzer, C. Ozga, C. Richter, J. Rist, M. Schöffler, D. Trabert, I. Vela-Perez, J. H. Viehmann, M. Weller, R. Dörner *et al.*, Mechanisms of one-photon two-site double ionization after resonant inner-valence excitation in Ne clusters, Phys. Rev. Res. **5**, 013055 (2023).

[38] S. Eckart, Strong field-induced quantum dynamics in atoms and small molecules, J. Phys. B **57**, 202001 (2024).

[39] R. Dörner, V. Mergel, O. Jagutzki, L. Spielberger, J. Ullrich, R. Moshammer, and H. Schmidt-Böcking, Cold target recoil ion momentum spectroscopy: A 'momentum microscope' to view atomic collision dynamics, Phys. Rep. **330**, 95 (2000).

[40] Q. Liao, P. Lu, Q. Zhang, W. Hong, and Z. Yang, Phase-dependent nonsequential double ionization by few-cycle laser pulses, J. Phys. B **41**, 125601 (2008).

[41] H. Liu, H. Zhang, X. Wang, and J. Yuan, Atomic double ionization with quantum light, Phys. Rev. Lett. **134**, 123202 (2025).

[42] K. Patkowski, G. Murdachaew, C. M. Fou, and K. Szalewicz, Accurate *ab initio* potential for argon dimer including highly repulsive region, Mol. Phys. **103**, 2031 (2005).

[43] A. Becker and F. H. M. Faisal, Correlated Keldysh-Faisal-Reiss theory of above-threshold double ionization of He in intense laser fields, Phys. Rev. A **50**, 3256 (1994).

[44] H. Ni, S. Chen, C. Ruiz, and A. Becker, Selection rules in the few-photon double ionization of the helium atom, J. Phys. B **44**, 175601 (2011).

[45] M. Y. Amusia, E. G. Drukarev, and E. Z. Liverts, Back-to-back emission of the electrons in double photoionization of helium, JETP Lett. **96**, 70 (2012).

[46] X. Ma, M. Li, Y. Zhou, and P. Lu, Nonsequential double ionization of Xe by mid-infrared laser pulses, Opt. Quantum Electron. **49**, 170 (2017).

[47] H. R. Larsson and D. J. Tannor, Control of concerted back-to-back double ionization dynamics in helium, J. Chem. Phys. **155**, 144105 (2021).

[48] K. Henrichs, S. Eckart, A. Hartung, D. Trabert, K. Fehre, J. Rist, H. Sann, M. Pitzer, M. Richter, H. Kang, M. S. Schöffler, M. Kunitski, T. Jahnke, and R. Dörner, Multiphoton double ionization of helium at 394 nm: A fully differential experiment, Phys. Rev. A **98**, 043405 (2018).

[49] R. R. Freeman, P. H. Bucksbaum, H. Milchberg, S. Darack, D. Schumacher, and M. E. Geusic, Above-threshold ionization with subpicosecond laser pulses, Phys. Rev. Lett. **59**, 1092 (1987).

[50] H. Ni, Long-range electron correlation in dissociative double ionization of argon dimers, Zenodo (2025), https://doi.org/10.5281/zenodo.15686321.

[51] D. Bohm, A suggested interpretation of the quantum theory in terms of "hidden" variables. I, Phys. Rev. **85**, 166 (1952).

[52] D. Bohm, A suggested interpretation of the quantum theory in terms of "hidden" variables. II, Phys. Rev. **85**, 180 (1952).